High-temperature superconducting filter using self-embedding asymmetric stepped impedance resonator with wide stopband performance and miniaturized size*

Dan Wang(王丹)[1], Bin Wei(魏斌)[1,†], Yong Heng(衡勇)[2], and Bi-Song Cao(曹必松)[1]

[1] *State Key Laboratory of Low-Dimensional Quantum Physics, Department of Physics, Tsinghua University, Beijing* 100084, *China*
[2] *Beijing Institute of Electronic System Engineering, Beijing* 100854, *China*

(Received 28 April 2017; revised manuscript received 12 June 2017; published online 10 September 2017)

In this study, a novel self-embedding asymmetric stepped impedance resonator (SE-ASIR) topology is proposed. By embedding asymmetric stepped impedance resonators in themselves, circuit sizes of ASIRs can be reduced effectively, while the ability to control spurious modes of ASIRs remains. Therefore, SE-ASIRs are suitable for being used to design filters with wide stopbands and miniaturized sizes. Furthermore, the construction process of the SE-ASIR is described in detail, and an equivalent model of the SE-ASIR is proposed. For demonstration, a high-temperature superconducting bandpass filter centered at 1112 MHz is designed and fabricated. The measured result agrees well with the simulation result and shows that the out-of-band rejection is better than 60 dB up to 4088 MHz, which is about 3.7 times the center frequency. The filter circuit size is 31 mm $\times$13 mm or $0.28\lambda_g \times 0.12\lambda_g$, where λ_g is the guided wavelength at 1112 MHz.

Keywords: high-temperature superconducting, bandpass filter, microstrip filter, wide stopband

PACS: 85.25.–j **DOI:** 10.1088/1674-1056/26/10/108502

1. Introduction

Microstrip filters are extensively used in modern wireless communications systems because of their simple fabricating procedures and compact sizes.[1–3] However, as planar devices, microstrip filters suffer unwanted spurious bands.[4] To solve this problem, bandpass filters with small sizes, wide stopbands and high rejection levels are demanded. Many resonators have been proposed to construct wide stopband filters, such as half-wavelength resonators,[5] quasi-lumped element resonators,[6] modified line resonators,[7] defected grounded structures resonators,[8] and stepped-impedance resonators (SIRs).[9–14]

Among the methods, SIRs are attractive due to simple theoretical models and convenient fabrications. The basic principle of SIRs is presented in Ref. [9]. The fundamental frequency f_0 and the first spurious frequency f_s of an SIR can be tuned by adjusting the structural parameters of SIR, and the f_s/f_0 ratio of an SIR is proportional to its impedance ratio. As a result, to shift up the f_s/f_0 ratio of SIRs, low impedance lines of SIRs are usually large, which restricts the application of SIRs. To address this issue, several methods have been developed to reduce the circuit size or further enhance the spurious suppression features of SIR filters. Introducing transmission zeros is a popular method to improve wide stopband performance.[10–13] In Refs. [10]– [12], transmission zeros are introduced by tapping stubs on SIR filters. In Ref. [13], couplings between SIRs are used to provide transmission zeros. These transmission zeros are properly located to attenuate the spurious harmonics of filters. Because the transmission zeros cannot eliminate spurious frequencies directly, the stopbands of these filters are usually wide but not very deep. At the same time, grounded quarter-wavelength structures are also used to design wide stopband SIR filters,[5,14,15] because the grounding can reduce circuit sizes and eliminate the even order spurious harmonics of SIR filters simultaneously. For example, in Ref. [15], stub-loaded SIRs with multiple transmission zeros and quarter-wavelength are proposed to design wide stopband filters. However, the grounding structures will increase the insertion loss and fabrication difficulty of a filter. In addition, use of multi-layers structures are beneficial to the decrease of circuit sizes of SIR filters. For example, in Ref. [16], SIRs are embedded on the middle layer of a bandpass filter, which can achieve spurious suppression, with no modification of the entire circuit size. However, the fabrication of multi-layer filters are usually difficult.

Recently, the interest in planar asymmetric SIR (ASIR) wide stopband filters has been aroused. ASIRs are used to enhance the spurious suppression performances of multi-bands filters[17,18] or construct wide stopband filters.[19–21] Compared with conventional symmetric SIRs, ASIRs can control spurious modes as symmetric SIRs while occupying smaller circuit sizes.

On the other hand, because of characteristics of low inser-

*Project supported by the National Natural Science Foundation of China (Grant No. 61371009) and the National High Technology Research and Development Program of China (Grant No. 2014AA032703).

†Corresponding author. E-mail: weibin@mail.tsinghua.edu.cn

© 2017 Chinese Physical Society and IOP Publishing Ltd

tion loss, high out-of-band rejection, and high selectivity,[22,23] high-temperature superconducting (HTS) filters have been widely used to fabricate high-performance radio-frequency front end or microwave devices,[24–27] including wide stopband filters.[6,7,10,19]

In this work, a novel self-embedding ASIR (SE-ASIR) with miniaturized size and controllable spurious harmonics is proposed. The topology of the SE-ASIR is derived from conventional ASIR. The SE-ASIR has an advantage of miniaturized size over conventional ASIR with one discontinuity, but can push its spurious harmonics higher than it. The construction process of the SE-ASIR is described in detail, through two topology transformations. Furthermore, an equivalent model of the SE-ASIR is proposed. Finally, for demonstration, a small HTS filter is designed and fabricated using the SE-ASIR. The measurements of the filter agree well with simulations, and exhibit good spurious suppression performance in terms of both wide stopband and high rejection level.

2. Resonator design

2.1. Structure and resonant characteristics of SE-ASIR

The structure of the proposed SE-ASIR is shown in Fig. 1. It is composed of three segments with different impedances: a low-impedance rectangle patch (segment A), a high-impedance spiral line (segment B) and a hollow patch (segment C). By embedding the large segment A in the hollow segment C, the circuit size of SE-ASIR is much smaller than a conventional SIR.

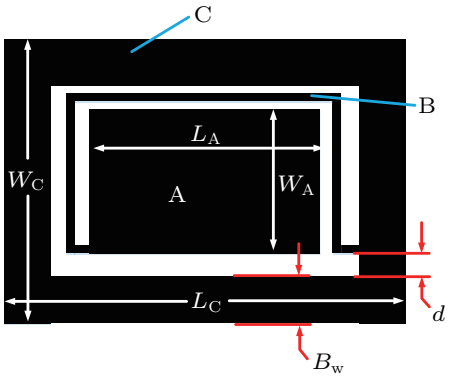


Fig. 1. (color online) Structure of SE-ASIR.

Meanwhile, the spurious suppression performance of SE-ASIR is better than that of conventional ASIR with one discontinuity. Figure 2 shows that the spurious resonance frequencies of SE-ASIR can be manipulated by changing the width W_A and length L_A of segment A. The larger the parameters W_A and L_A, the higher the f_s/f_0 is. And when W_A increases to 3 mm, i.e., $Z_B/Z_A = 6.2$, the f_s/f_0 can be increased to be higher than 3.8, which is much larger than the ratio of conventional ASIR with two step discontinuities. According to the analyses in Refs. [19] and [20], even when the impedance ratio Z_B/Z_A of a conventional ASIR with one discontinuity is as high as 10, the maximum f_s/f_0 ratio is still smaller than 3.0.

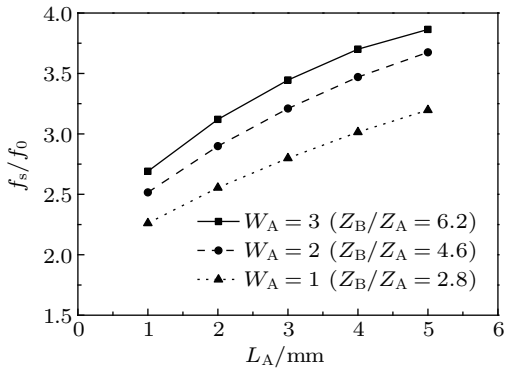


Fig. 2. Plots of simulated f_s/f_0 versus length L_A of SE-ASIRs for different values of line width W_A with $L_C = 8.28$ mm and $W_C = 5.84$ mm.

2.2. Construction process of SE-ASIR

The topology of SE-ASIR is derived from conventional ASIR with two discontinuities. The resonant properties of SE-ASIR can be analyzed by using the equivalent model, which is an ASIR as shown in Fig. 3. However, this equivalent model is not very intuitive. Thus, in this subsection, two topology transformations (shown in Fig. 4) and the corresponding conditions are discussed in detail, to describe the construction process of the equivalent model. And figure 4 shows that the circuit size of Topology I is about 60% of that of Topology III.

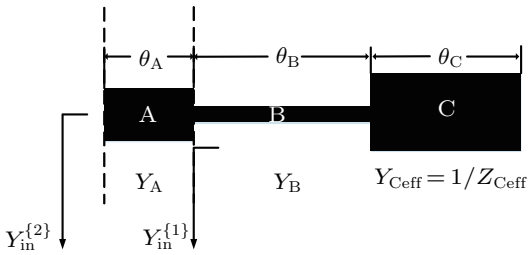


Fig. 3. Equivalent model of SE-ASIR.

Topology I is the original topology of SE-ASIR. It can be divided into two parts: the interior, which is printed in blue, and the exterior, which is printed in black as shown in Fig. 4(a). Topology II is constructed by taking the inner part of Topology I out and tapping this part on the outside edge of the exterior as shown in Fig. 4(b).

Resonant characteristics of Topology I and Topology II are equal, on condition that the inner blue part and the black exterior part of Topology I are far apart. This conclusion is verified by the EM simulations shown in Fig. 5. Actually, it is seen that when the gap distance d between the inner part and exterior part is 0.48 mm, the maximum deviations of f_0 and f_s between Topology I and Topology II are only 0.9% and 1.4%, respectively. And when gap distance d decreases to 0.04 mm, the maximum deviations of f_0 and f_s between the two topologies increase to 5.5% and 8.1%, respectively.

Besides, it is worthy to mention that when d decreases from 0.48 mm to 0.04 mm, f_0 of SE-ASIR topology decreases and f_s of SE-AISR increases, thereby increasing f_s/f_0, as shown in Fig. 5. Nevertheless, the gap distance d is still set to be 0.48 mm in this work, to ensure that Topology I and Topology II exhibit equally resonant patterns.

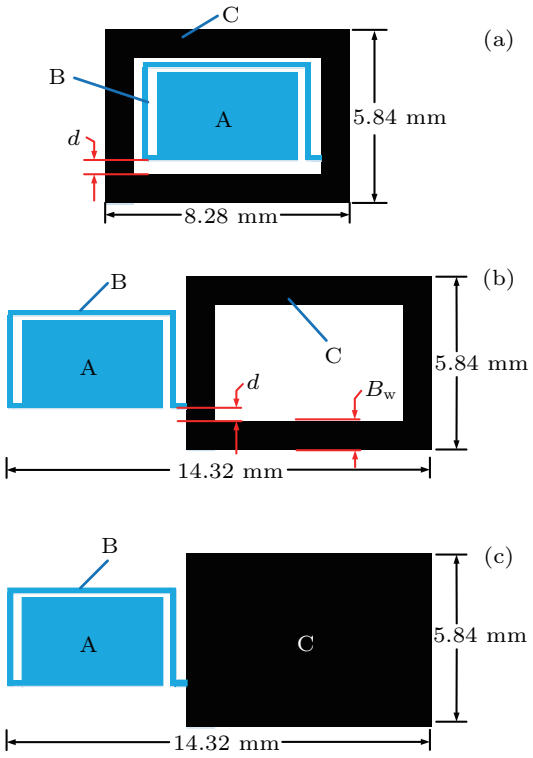


Fig. 4. (color online) (a) Topology I, topology of SE-ASIRs, (b) Topology II, topology of hollow ASIRs, and (c) Topology III, topology of folded ASIRs.

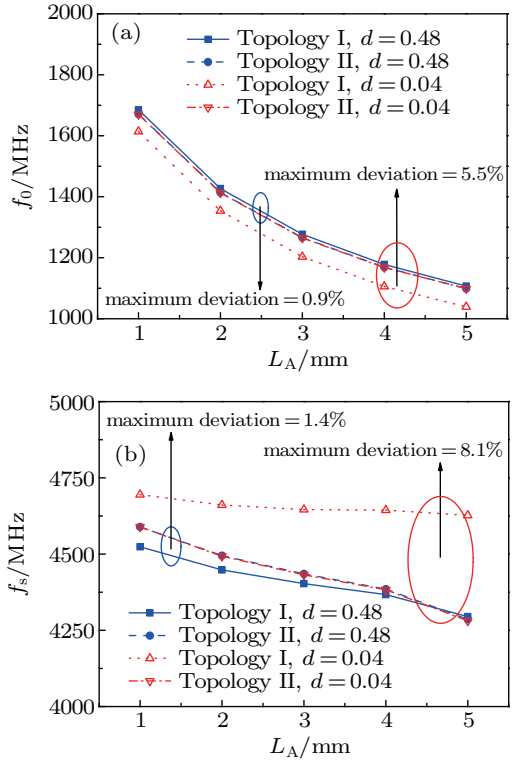


Fig. 5. (color online) Deviations of resonant frequencies between Topology I and Topology II at (a) fundamental frequency f_0 and (b) the first spurious frequency f_s.

The above effect of gap distance d on resonant frequency is caused by the self-capacitance between the interior and exterior of SE-ASIR. The current and charge distributions of SE-ASIR at f_0 and f_s are plotted in Fig. 6. Like traditional half-wavelength straight resonators, unlike and like charges concentrate at the two ends of SE-ASIR at f_0 and f_s, respectively. In Topology I, the two ends of ASIR are very close, especially when the gap distance d is small. In such a situation, the unlike charges on the two ends of SE-ASIR will enlarge the self-capacitance of the area surrounded by the dash line in Fig. 5(c). At f_s, the like charges will diminish the elf-capacitance. According to the expression $f = 1/\sqrt{2\pi LC}$, the larger self-capacitance C at f_0 will reduce the fundamental frequency, and the smaller self-capacitance C at f_s will diminish the spurious frequency. Therefore, as illustrated in Fig. 5, the resonant frequencies of Topology I and Topology II have the following relationships:

$$f_0 \text{ (Topology II)} \approx f_0 \text{ (Topology I, } d = 0.48 \text{ mm)} > f_0 \text{ (Topology I, } d = 0.04 \text{ mm)},$$

$$f_s \text{ (Topology II)} \approx f_0 \text{ (Topology I, } d = 0.48 \text{ mm)} < f_0 \text{ (Topology I, } d = 0.04 \text{ mm)}.$$

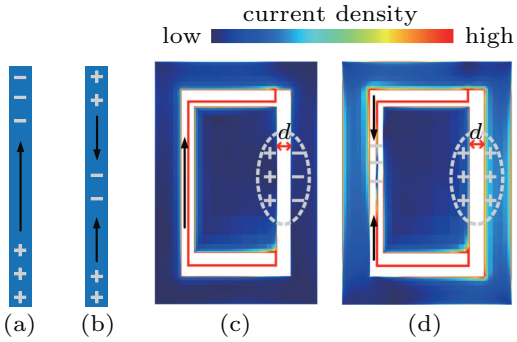


Fig. 6. (color online) Current and charge distributions of (a) a straight-line resonator at f_0, (b) a straight-line resonator at f_s, (c) SE-ASIR at f_0, and (d) SE-ASIR at f_s.

The topology transformation from Topology II to Topology III is also studied. The two topologies have similar resonant patterns. Topology III is a folded conventional ASIR, which is constructed through replacing the hollow segment C of Topology II by a solid one as shown in Fig. 4(c). As a result of skin effect, almost no current is present in the central area of the large microstrip patch segment C of Topology III. Thus, the absence of the central area will not change the basic resonant pattern of the large microstrip patch of Topology III. EM simulations support this conclusion. As shown in Fig. 7, the resonant frequencies curves of Topology II with different values of border width B_w have the same trend as those of Topology III. When the border width B_w increases to 2.4 mm, the resonant frequencies of Topology II and Topology III are almost the same.

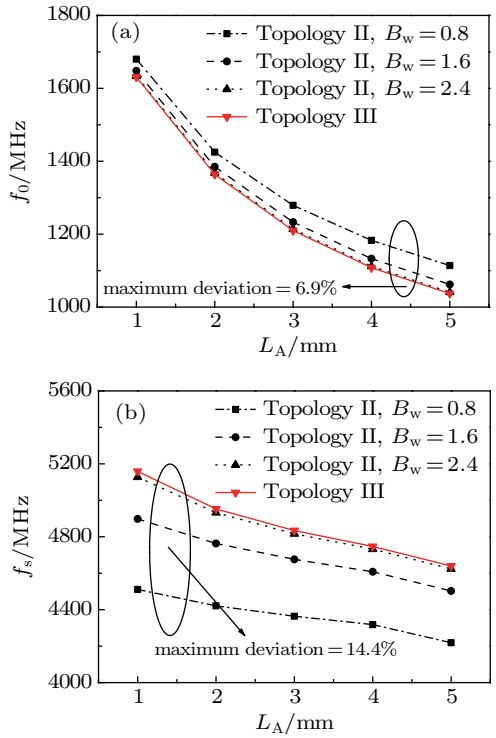


Fig. 7. (color online) Deviations of resonant frequencies between Topology II and Topology III at (a) fundamental frequency f_0 and (b) the first spurious frequency f_s.

2.3. Equivalent model of SE-ASIR

Through the above discussion, it is known that an SE-ASIR can be equivalent to the ASIR model in Fig. 3. Considering the deviation between Topology II and Topology III, the hollow segment C of SE-ASIR is equivalent to a microstrip line with characteristic impedance Z_{Ceff}. Z_{Ceff} is larger than Z_{C}, which is the characteristic impedance of a solid patch with the same size as the hollow segment C.

On the basis of the model, the resonant frequencies f_0 and f_s of SE-AISR can be obtained from the transmission line theory.[28] The input admittance $Y_{\text{in}}^{\{2\}}$ of the proposed SE-ASIR is derived as

$$Y_{\text{in}}^{\{2\}} = \text{j}Y_A \frac{Y_{\text{in}}^{\{1\}} + Y_A \tan(\theta_A)}{Y_A - Y_{\text{in}}^{\{1\}} \tan(\theta_A)}, \tag{1}$$

in which

$$Y_{\text{in}}^{\{1\}} = \text{j}Y_{\text{B}} \frac{Y_{\text{Ceff}} \tan(\theta_{\text{C}}) + Y_{\text{B}} \tan(\theta_{\text{B}})}{Y_{\text{B}} - Y_{\text{Ceff}} \tan(\theta_{\text{B}}) \tan(\theta_{\text{C}})}. \tag{2}$$

Under the resonant condition $Y_{\text{in}}^{\{2\}} = 0$, the resonant frequencies of the SE-ASIR can then be calculated by employing a simple root-searching program. For example, in this work, dielectric constant $\varepsilon_{\text{e}} = 9.74$, $Z_{\text{A}} = 15.53\ \Omega$, $Z_{\text{B}} = 95.86\ \Omega$, and $\theta_{\text{C}}/\theta_{\text{B}} = 0.75$, the resonant frequency ratio f_s/f_0 against $u = \theta_{\text{A}}/(\theta_{\text{A}} + \theta_{\text{B}})$ under different values of Z_{Ceff} are calculated and plotted in Fig. 8. Notably, when $u < 0.5$, the ratio f_s/f_0 increases with a growing θ_{A}, which accords with the plots in Fig. 2. And when $u = 0$, which means that the ASIR is reduced to a conventional ASIR with two step discontinuities, and the f_s/f_0 is smaller than 3. The extreme f_s/f_0 of the SE-ASIR occurs at $u \approx 0.5$. In addition, figure 8 shows that a smaller Z_{Ceff} corresponds to a higher f_s/f_0 ratio.

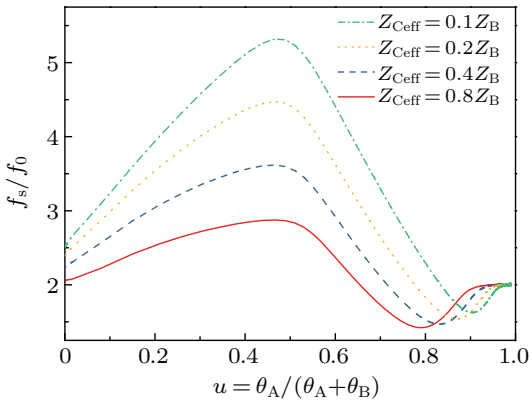


Fig. 8. (color online) Ratios of f_s/f_0 versus u of SE-ASIR for different values of $Z_{\text{Ceff}}/Z_{\text{B}}$.

Our objective is to obtain a large ratio of f_s/f_0 and a small circuit size. Figure 8 shows that when $u < 0.5$, the f_s/f_0 increases with growing θ_{A} and Z_{Ceff}. However, the increases in θ_{A} and Z_{Ceff} will also increase the whole size of SE-ASIR. Taken together, in this work, parameter u is approximately 0.3, and parameter Z_{C} is approximately 0.1 Z_{B}. The f_s/f_0 of the designed SE-ASIR is 3.8, which indicates that real Z_{Ceff} is about 0.2 Z_{B}, according to Fig. 8.

2.4. Coupling properties of SE-ASIR

There are three kinds of resonator coupling patterns for SE-ASIR as shown in Fig. 9. Because their different inner parts are embedded in the same hollow large patch of SE-ASIR and will not influence the adjacent coupling, and their coupling coefficients are similar. This coupling property is convenient for filter design.

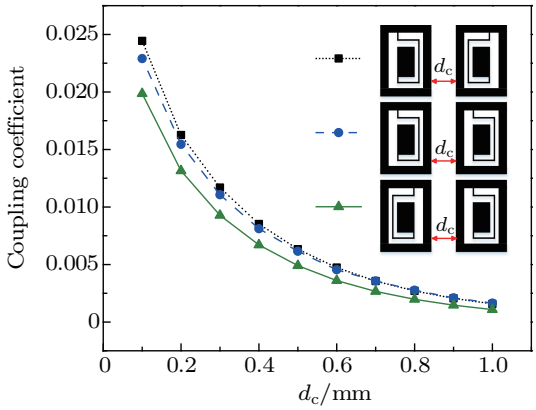


Fig. 9. (color online) Three kinds of coupling patterns of SE-ASIR at 1112 MHz.

3. Filter design, fabrication, and measurements

For demonstration, a four-pole Chebyshev bandpass filter is designed using the proposed SE-ASIRs. The center fre-

quency and bandwidth of the filter are chosen as 1112 MHz and 10 MHz, respectively. On the basis of these settings, the resonator parameters of the proposed filter are determined, which are $W_A = 2.96$, $L_A = 4.76$, $W_B = 0.08$, $L_B = 13.14$, $L_C = 8.28$, $W_C = 5.84$, $d = 0.48$, and $B_w = 0.96$ (all in unit mm) as shown in Fig. 1. The W_B and L_B are the width and whole length of the segment B of SE-ASIR, respectively. The coupling coefficients and external quality factor of the filter are obtained by using the standard design procedure in Ref. [28], which are, $k_{12} = k_{34} = 0.0097$, $k_{23} = 0.0071$, and $Q_e = 79.34$. Then, the other physical parameters of the filter are determined as follows: $l_1 = 2.82$, $l_2 = 5.98$, $l_3 = 6.16$, $l_4 = 31.00$, $l_5 = 13.00$, $w_1 = 0.48$, $w_2 = 0.24$, $g_1 = 0.08$, $d_{12} = 0.44$, $d_{23} = 0.48$, and $h_{12} = 0.82$ (all in unit mm) as shown in the following Fig. 10.

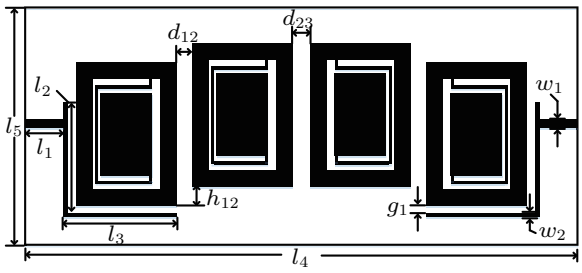


Fig. 10. Layout of SE-ASIR filter.

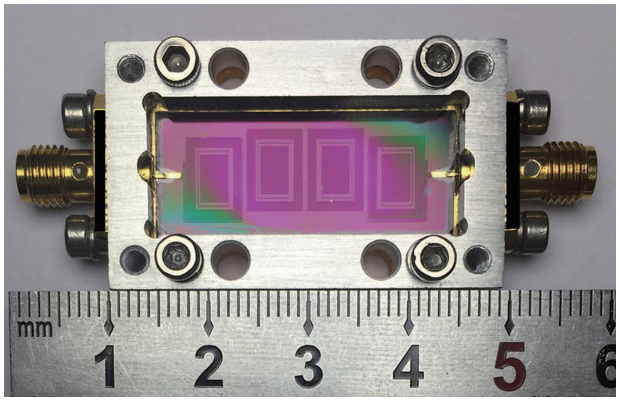


Fig. 11. (color online) Photograph of fabricated filter with top cover removed.

The filter is fabricated on a double-sided YBCO film with a relative dielectric constant of 9.74 and a thickness of 0.50 mm, deposited on an MgO substrate. The filter size is 31 mm $\times$13 mm or $0.28\lambda_g \times 0.12\lambda_g$, where λ_g is the guided wavelength at 1112 MHz. A photograph of the fabricated HTS filter is shown in Fig. 11.

The fabricated HTS filter is cooled to 60 K and measured using an Agilent E5072A network analyzer with an input power of 0 dBm. The measurement agrees well with the simulation. As shown in Fig. 12, the filter is centered at 1112 MHz with a 3-dB fractional bandwidth of 10 MHz. The maximum insertion loss is 0.12 dB and the return loss is better than 20 dB. As shown in Fig. 13, the stopband rejection of the filter is better than 60 dB up to 4088 MHz, which is approximately 3.7 times the fundamental frequency. The performance of the fabricated filter is summarized and compared with those of other SIR filters as shown in Table 1. The filter in this work exhibits wide stopband, high rejection level and small circuit size simultaneously.

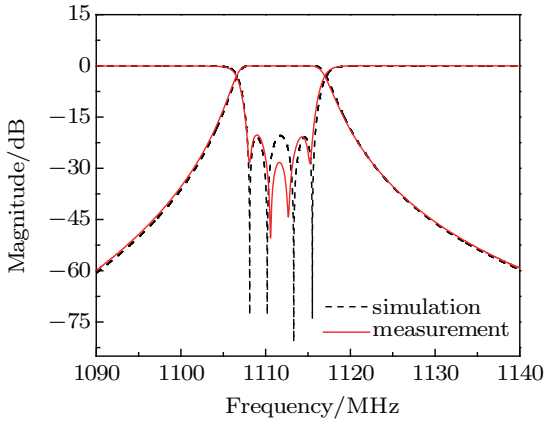


Fig. 12. (color online) Simulated and measured narrow-band responses of the proposed HTS filter.

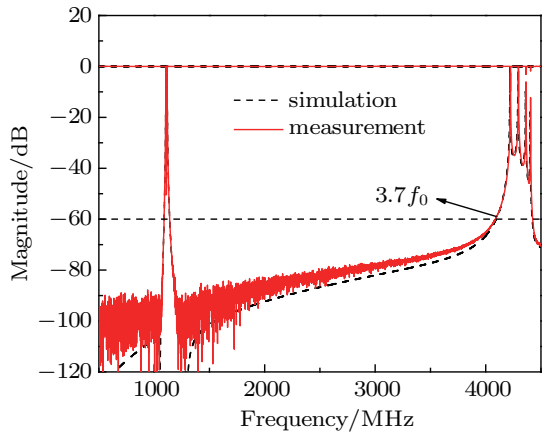


Fig. 13. (color online) Simulated and measured wide-band responses of the proposed HTS filter.

Table 1. HTS wide stopband filter comparisons.

Ref.	Topology	Poles	f_0/GHz	3-dB-FBW/%	Size (λ_g)	Rejection up to
[10]	SIR	4	7.4	2.2	1.45×0.48	(70 dB) 2.3 f_0
[19]	ASIR	4	2.4	10.3	0.47×0.26	(20 dB) 4.4 f_0
[20]	ASIR	2	1.5	8.9	0.16×0.12	(24 dB) 10.6 f_0
This work	SE-ASIR	4	1.1	0.9	0.28×0.12	(60 dB) 3.7 f_0

The filters in Refs. [10], [19] and this work are all HTS filters.

4. Conclusions

In this article, we present a novel self-embedding SIR structure. This resonator structure can shift the spurious harmonics to higher than 3.7 times the fundamental frequency while occupying a miniaturized circuit size. For demonstration, an HTS bandpass filter with wide stopband, high rejection level and small size is designed and fabricated using the proposed SIRs. The measurement agrees well with the simulation.

References

[1] Zhang Q S, Zhu F J and Zhou H S 2015 *Chin. Phys. B* **24** 107506
[2] Liu X Y, Zhu L and Feng Y J 2016 *Chin. Phys. B* **25** 034101
[3] Zeng Z, Yao Y and Zhuang Y 2015 *Acta Phys. Sin.* **64** 164101 (in Chinese)
[4] Chang C Y and Itoh T 1991 *IEEE Trans. Microw. Theory Techniq.* **39** 310
[5] Lin S, Deng P, Lin Y, Wang C and Chen C H 2006 *IEEE Trans. Microw. Theory Techniq.* **54** 1011
[6] Wang D, Wei B, Cao B, Chen J, Zhen T and Gao T 2015 *IEEE Microw. Wireless Compon. Lett.* **25** 703
[7] Ying Z, Guo X, Cao B, Zhang X, Wei B, Zhang Y, Li Q, Feng C, Song X, Heng Y and Zhang G 2013 *IEEE Trans. Appl. Supercond.* **23** 1500706
[8] Luo X, Ma J, Li E and Ma K 2011 *IEEE Trans. Electromagn. Compat.* **53** 717
[9] Mitsuo M and Sadahiko Y 1980 *IEEE Trans. Microw. Theory Techniq.* **28** 1413
[10] Li Q, Guo X, Zhang X, Wei B, Chen W, Zhang Y, Feng C, Yin Z, Jin S and Cao B 2012 *Physica C* **483** 5
[11] Jen-Tsai K and Erik S 2003 *IEEE Trans. Microw. Theory Techniq.* **51** 1554
[12] Tang C and Chen M 2006 *IEEE Microw. Wireless Compon. Lett.* **16** 666
[13] Kongpop U, Edward J W, Terence A D, John P and Joy L 2006 *IEEE Trans. Microw. Theory Techniq.* **54** 1237
[14] Kuo T N, Li W C, Wang C H and Chen C H 2008 *IEEE Microw. Wireless Compon. Lett.* **18** 389
[15] Xu J, Ji Y X, Miao C and Wu W 2013 *IEEE Microw. Wireless Compon. Lett.* **23** 338
[16] Kuan H, Lin Y L, Yang R Y and Chang Y C 2010 *IEEE Microw. Wireless Compon. Lett.* **20** 25
[17] Wu H W and Yang R Y 2011 *IEEE Microw. Wireless Compon. Lett.* **21** 203
[18] Kim C H and Chang K 2011 *IEEE Trans. Microw. Theory Techniq.* **59** 3037
[19] Liu H, Ren B, Li S, Guan X, Wen P, Xiao X and Peng Y 2015 *IEEE Trans. Appl. Supercond.* **25** 1501606
[20] Kim C H and Chang K 2013 *IEEE Microw. Wireless Compon. Lett.* **23** 69
[21] Chang Y C, Kao C H, Weng M H and Yang R Y 2008 *IEEE Microw. Wireless Compon. Lett.* **18** 770
[22] Raafat R M 2002 *IEEE Trans. Microw. Theory Techniq.* **50** 750
[23] Li H C, Wang R L, Wei B and Zhen D N 2005 *Acta Phys. Sin.* **54** 359 (in Chinese)
[24] Sun L and He Y 2014 *IEEE Trans. Appl. Supercond.* **24** 1501308
[25] Gao T, Wei B and Heng Y 2017 *Chin. Phys. B* **26** 058503
[26] Zuo T, Zhao X J, Wang X K, Yue H W, Fang L and Yan S L 2009 *Acta Phys. Sin.* **58** 4194 (in Chinese)
[27] Cui B, Zhang X Q, Sun L, Bian Y B, Guo J, Wang J, Li C G, Li H, Zhang Q and He Y S 2010 *Sci. Bull.* **55** 1367
[28] Hong J S 2011 *Microstrip Filters for RF/microwave Applications*, 2nd edn. (New York: Wiley)